Ultrasonics Sonochemistry 20 (2013) 872–880

Contents lists available at SciVerse ScienceDirect

Ultrasonics Sonochemistry

journal homepage: www.elsevier.com/locate/ultson

Sonochemical fabrication of Fe_3O_4 nanoparticles on reduced graphene oxide for biosensors

Shenmin Zhu [a,*], Jingjing Guo [a], Junping Dong [b], Zhaowen Cui [a], Tao Lu [a], Chenglin Zhu [a], Di Zhang [a,*], Jun Ma [c]

[a] State Key Lab of Metal Matrix Composites, Shanghai Jiao Tong University, 800 Dongchuan Road, Shanghai 200240, PR China
[b] Department of Chemistry, College of Science, Shanghai University, Shanghai 200444, PR China
[c] School of Advanced Manufacturing & Mechanical Engineering, University of South Australia, Mawson Lakes, SA 5095, Australia

ARTICLE INFO

Article history:
Received 26 July 2012
Received in revised form 30 November 2012
Accepted 2 December 2012
Available online 11 December 2012

Keywords:
Ultrasonication
Fe_3O_4 nanoparticles
Graphene
Biosensor

ABSTRACT

This study synthesized Fe_3O_4 nanoparticles of 30–40 nm by a sonochemical method, and these particles were uniformly dispersed on the reduced graphene oxide sheets (Fe_3O_4/RGO). The superparamagnetic property of Fe_3O_4/RGO was evidenced from a saturated magnetization of 30 emu/g tested by a sample-vibrating magnetometer. Based on the testing results, we proposed a mechanism of ultrasonic waves to explain the formation and dispersion of Fe_3O_4 nanoparticles on RGO. A biosensor was fabricated by modifying a glassy carbon electrode with the combination of Fe_3O_4/RGO and hemoglobin. The biosensor showed an excellent electrocatalytic reduction toward H_2O_2 at a wide, linear range from 4×10^{-6} to 1×10^{-3} M ($R^2 = 0.994$) as examined by amperometry, and with a detection limit of 2×10^{-6} M. The high performance of H_2O_2 detection is attributed to the synergistic effect of the combination of Fe_3O_4 nanoparticles and RGO, promoting the electron transfer between the peroxide and electrode surface.

1. Introduction

Hydrogen peroxide (H_2O_2) is essential in numerous applications, particularly in food, biological, medicine and environmental industries. Therefore, it is of significance to accurately gauge the H_2O_2 concentration using cost-effective approaches. Electrochemically sensing H_2O_2 is considered as the most promising method due to its cost-effective fabrication and high sensitivity and suitability for real-time detection [1]. Carbon is a major material used as solid electrodes. Carbon nanotube-modified electrodes have been widely recognized as the ideal material for electrocatalyzing H_2O_2. By contrast, graphene is more suitable due to its unique features including extremely high surface area, striking mechanical stiffness, extraordinary electronic transportation and good biocompatibility. The modification of electrodes by electrically conductive, cost-effective graphene is promising for the development of biosensors, since graphene can provide a favorable microenvironment for enzyme and promote a direct electron transfer of enzyme at the modified electrodes [2–5].

The first crucial factor in biosensor fabrication is the immobilization of enzymes using metal nanoparticles to retain bioactivity. Enzymes showed an increase in the electron transfer and biocatalytic activity when they were adsorbed on nanomaterials [6]. Many types of metal oxide nanoparticles, such as copper oxide [7], zinc oxide [8], titanium oxide [9] and zirconium oxide [10], have been developed to improve the efficiency of immobilization; of these nanoparticles, magnetite (Fe_3O_4) nanoparticles have been widely used in biomagnetic fields, such as separation of biochemical products, magnetic resonance imaging, targeted drug delivery and biosensing, due to their superior biocompatibility, super paramagnetic property and more importantly, the intimate contact among the nanoparticles, biocatalyst and substrates [11–13]. Fe_3O_4 nanoparticles are indeed considered as an effective carrier for immobilization of desired biomolecules for biosensing.

However, agglomeration prevents Fe_3O_4 nanoparticles effectively immobilizing proteins and enzymes. Thus, the second crucial factor in biosensor fabrication is to uniformly disperse these nanoparticles in a suitable matrix such as chitosan, carbon and graphene to prevent agglomeration. Nanoparticles of ferric oxides (hematite, magnetite) have been incorporated into carbon paste, which exhibited superior electrocatalytic properties for H_2O_2 reduction [14]. It is of great interest to modifying electrodes with the combination of graphene with magnetic Fe_3O_4 particles for constructing novel biosensors.

Generally, a Fe_3O_4/graphene composite is synthesized by *in situ* reduction of ferric hydroxide [15] or by microwave heating [16], both of which are disadvantaged by either large particle sizes or poor particle dispersion, and thus special treatments or equipment are needed to address these disadvantages. In order to fabricate the uniformly dispersed Fe_3O_4 nanoparticles on graphene sheets, Hsieh reported a sonochemical method, which can dispersed Fe_3O_4 nano-

* Corresponding authors. Tel.: +86 21 34202584; fax: +86 21 34202749.
E-mail addresses: smzhu@sjtu.edu.cn (S. Zhu), zhangdi@sjtu.edu.cn (D. Zhang).

1350-4177/$ - see front matter © 2012 Elsevier B.V. All rights reserved.
http://dx.doi.org/10.1016/j.ultsonch.2012.12.001

particles of ~10 nm in diameter on the reduced graphene sheet [17]. Unfortunately, Fe_3O_4 co-existed with Fe_2O_3 in their study, owing to the use of a hydrogen reduction process. Meanwhile, Behera developed a method where a mixture of Fe_3O_4 and graphene oxide was created and then baked under inert atmosphere to fabricate a nanocomposite [18]. However, it is not clear whether these nanoparticles were uniformly dispersed or aggregated due to absence of TEM investigation, since it is well known that a simple mechanical mixture process cannot lead to a uniform dispersion of nanoparticles.

Recently, Fe_3O_4/graphene composites have been prepared for immobilizing horseradish peroxidase (HRP) to construct a mediator-free H_2O_2 biosensor, wherein Fe_3O_4 particles of 200–250 nm in diameter were fabricated [19]. Nanoscale is extremely important for developing composite-based biosensors because nanoparticles exhibit far larger surface/volume ratio, much lower particle–particle distance and stronger adsorption ability than their peer micron-sized particles [20]. Developed approaches to fabricating smaller Fe_3O_4 nanoparticles on reduced graphene mainly include (i) chemical method to deposit Fe_3O_4 nanoparticles onto GO through adjusting pH, dialysis, ion exchange and precipitation [21], (ii) conjugation chemistry [22] and (iii) controlled assembly of Fe_3O_4 nanoparticles on GO. Method (iii) is more advantageous in controlling the fabrication of nanoparticles since it is able to functionalize GO using polyetheylenimine (PEI) and meso-2,3-dimercaptosuccinnicacid (DMSA) [21]. Unfortunately, these processes are complicated due to their multi-step procedures with expensive raw materials used. Therefore, it is a great challenge to cost-effectively fabricate and manipulate these nanoparticles on graphene to achieve a uniform dispersion.

Ultrasonication has proved effective in generating nanoparticles of attractive properties with a short reaction time, due to acoustic cavitation phenomena. The extremely high local temperature (>5000 K), pressure (>20 MPa) and very high cooling rates (>1010 K S^{-1}) confer sonicated solutions unique properties, which can reduce metal ions to metal or metal oxide nanoparticles [23]. This method features a simple and energy-efficient process. Herein, we present a sonochemical approach to fabricating Fe_3O_4 nanoparticles and uniformly dispersing these on the surface of graphene oxide. After thermal reduction, Fe_3O_4 nanoparticles of 30–40 nm in diameter should disperse homogeneously on the reduced graphene oxide (Fe_3O_4/RGO). We then modify an electrode with Fe_3O_4/RGO. The electrocatalytic evaluation of our electrode displays a stable but highly sensitive response to the H_2O_2 reduction.

2. Experimental

2.1. Reagents and materials

Graphite powder and $FeCl_3{\cdot}6H_2O$ were purchased from Shanghai Chemical Reagent Co., Ltd. Hemoglobin (HB) and chitosan were purchased from Sigma and used without further purification. 30% H_2O_2 solution was purchased from Shanghai Lingfeng Chemical Reagent Co., Ltd, and a fresh H_2O_2 solution was prepared daily. All other chemicals were of analytical grade and used as received. 0.1 M phosphate buffer solution (PBS, pH 7) consisting of Na_2HPO_4 and NaH_2PO_4 was used as a supporting electrolyte. The ultra-pure water used to prepare all solutions was obtained from a water purification system provided by Shanghai Winner Environmental technology Co., Ltd.

2.2. Preparation of graphene oxide

Graphene oxide (GO) was prepared from natural graphite by a modified Hummers method. In specific, 2 g of graphite and 1 g of $NaNO_3$ were mixed with 46 mL of H_2SO_4 (98%) in a 250-mL wide-neck flask placed in an ice bath. Then, the mixture was stirred for 30 min. While maintaining vigorous magnetic stirring, a certain amount of $KMnO_4$ (6 g) was carefully added to the suspension. After that, the ice bath was replaced by an oil bath, and the mixture was stirred at 15 °C for 2 h. As the reaction progressed, the mixture gradually became pasty and the color turned into light brownish. The next step was to increase the reaction temperature to 40 °C and keep for another 1 h. Then, 92 mL of H_2O was slowly added to the pasty mixture with vigorous agitation. The reaction temperature was rapidly increased to 98 °C with effervescence, and the color changed to yellow. Finally, 30 mL of 5% H_2O_2 was added to the mixture and kept the high-temperature reaction going on for 1 h. For purification, the mixture was rinsed and centrifugated with deionized water for several times. After filtration and drying under vacuum at 60 °C, GO was obtained as a grey powder.

2.3. Preparation of Fe_3O_4/RGO nanocomposite

Fe_3O_4/RGO nanocomposite was synthesized by a sonochemical reduction of $FeCl_3{\cdot}6H_2O$ in the presence of GO. 0.10 g GO and 0.6 g $FeCl_3{\cdot}6H_2O$ was added to 20 mL ethanol and stirred for 12 h under vigorous magnetic stirring at ambient temperature. Then the suspension was sonicated at room temperature for 3 h under ultrasound power (in an ultrasonic bath with an input power and frequency of 100 W and 20 kHz, respectively. Hongxing Ultrasonic Co., Shanghai). Calorimetric measurement was employed to determine the acoustic power [24]. This method was used to calibrate the variable-frequency sonicator due to its simplicity and applicability. Each frequency was then calibrated for constant power by producing a number of heating curves at different input load powers and voltages [25]. The optimized reaction time was set at 3 h, because a long reaction time would result in a large amount of Fe_3O_4 on GO sheets. Finally the resulting composite was recovered by centrifugation and rinsed with ethanol and H_2O several times, and then dried under vacuum at 60 °C to obtain Fe_3O_4/GO composite. After calcination at 450 °C for 3 h under nitrogen, black Fe_3O_4/RGO was obtained. As a comparison, RGO denotes the GO that is thermally treated at the same temperature (450 °C for 3 h).

2.4. Characterization

The synthesized samples were characterized by X-ray diffraction (XRD) using a RigakuD/max2550VL/PC system operated at 40 kV and 40 mA with Cu-Kα radiation. Nitrogen adsorption measurements at 77 K were performed using an ASAP2020 volumetric adsorption analyzer, immediately after the samples had been degassed for 8 h in the degas port of the adsorption apparatus. Field-emission scanning electron microscopy (FE-SEM) was performed on a FEI Sirion 200 field emission gun scanning electron microscope (SEM) operated at 5.0 kV. Transmission electron microscopy (TEM) and energy-dispersive X-ray measurements (EDX) were carried out on a JEOL 2010 microscope at 200 kV. TEM specimens were prepared by grinding the synthesized samples into powders with a mortar and pestle, dispersing the powder in ethanol and dropping the suspension on holey carbon film-supported copper grids. A Dilor LABRAM-1B microspectrometer with 633 nm laser excitation was used to record the Raman spectrum of the samples. Fourier transform infrared measurements (FT-IR) were recorded on KBr pellets with a PE Paragon 1000 spectrophotometer. Thermal gravimetric analysis (TGA) was conducted on a PETGA-7 instrument with a heating rate of 20 °C min^{-1}. Diffuse reflectance electronic spectra (DRS) were measured with a Perkin–Elmer 330 spectrophotometer equipped with a 60-mm Hitachi integrating sphere accessory.

2.5. Electrochemical measurements

The glassy carbon electrode (GC, 3 mm in diameter) was polished to a mirror-like surface with 0.5 and 0.02 μm alumina slurry, sonicated in a mixture of nitric acid and ethanol (molar ratio 1:1), and washed by distilled water. Fe_3O_4/RGO (10 mg) was dispersed by sonication in 2-mL, pH = 7.0 PBS. 6 μL of the resulting homogeneous solution was spread evenly onto the well-polished glassy carbon electrodes and dried under an infrared lamp. Then, 2 μL Hb (5 mg/mL) was coated on the electrodes and allowed to dry at 4 °C. Finally, 2 μL Nafion (0.5 wt.%) was dropped on the electrode. If it was not used immediately, the electrode would be stored at 4 °C in a refrigerator.

Electrochemical measurements were carried out with a CHI 660C workstation (Chenhua, Shanghai, China) connected to a computer. A three-electrode configuration employed include: a modified glassy carbon electrode as the working electrode, Ag/AgCl (3 M KCl) as the reference electrode, and a platinum wire as the counter electrode.

3. Results and discussion

3.1. Composite characterization

Our Fe_3O_4/reduced graphene oxide (RGO) nanocomposite was fabricated by calcinating the Fe_3O_4/GO composite in nitrogen. In Fig. 1 where wide-angle X-ray diffraction (XRD) patterns of Fe_3O_4/RGO and Fe_3O_4/GO are compared, a diffraction at $2\theta = 11°$ in Fe_3O_4/GO is indexed as the (002) of GO, corresponding to a GO interlayer spacing 0.80 nm, much larger than that of pristine graphite (0.34 nm); and this is caused by loosely stacked GO, due to the presence of a great many oxygen-based groups and defects caused by the oxidation. A broad, intensive diffraction at $2\theta = 21°$ indicates that the iron compound existing in Fe_3O_4/GO is largely either FeOOH or $Fe(OH)_2$ in nature. Through calcination at 450 °C, the diffraction at $2\theta = 11°$ disappears and a new diffraction at $2\theta = 25°$ is assigned to graphene. During the thermal treatment, GO was partially reduced, as indicated by the strong diffraction $2\theta = 25°$. The remaining diffraction peaks in Fig. 1 are all assigned to the crystal planes of cubic Fe_3O_4 (JCPDS 75-0033), indicating that the Fe^{3+} precursors absorbed on GO were *in situ* reduced to crystalline Fe_3O_4 nanoparticles which were dispersed on the RGO surface after the thermal treatment. The average size of Fe_3O_4 in Fe_3O_4/RGO was calculated to be around 45 nm by using the Scherrer formula [26]. Our synthesis of ~45-nm Fe_3O_4 particles on RGO represents a great advance over previous efforts where either the synthesized particles are over 100 nm in diameter or the synthesis processes are too complicated [19]. This result demonstrates that the growth of crystalline Fe_3O_4 nanoparticles on RGO can be well manipulated by using ultrasonication, which will be further evidenced by the following TEM analysis. It is noted that a small amount of impurity was detected from XRD analysis, possibly due to the residue of FeOOH phase after calcination [27].

Fig. 2 shows Raman spectra of GO, RGO and Fe_3O_4/RGO. Their structures feature two absorptions: G-band at around 1595 cm^{-1} corresponding to a well defined sp^2 carbon-type structure and D-band at around 1350 cm^{-1} attributing to defects within the hexagonal graphitic structure. Thus a smaller I_D/I_G intensity ratio of a Raman spectrum indicates a lower defects and disorders of the graphitized structures. In Fig. 2, the reduction increases I_D/I_G from 0.95 for GO to 1.16 for RGO, suggesting that there were more defects in RGO after the treatment, similar phenomenon has been observed in elsewhere [28]. Nevertheless, the I_D/I_G of GO after the ultrasonication is 0.96, similar to that of GO (0.95), illustrating that ultrasonication has little effect on GO structure and it is the presence of Fe_3O_4 that reduces I_D/I_G down to 0.9. This demonstrates that GO is only reduced by thermal treatment with Fe_3O_4, resulting in a low degree of graphic lattice defects which would benefit its application as a biosensor. In Fig. 2 inset, three absorptions located

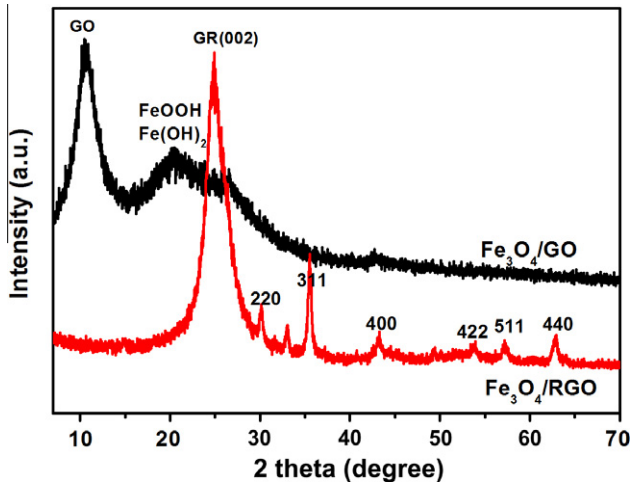

Fig. 1. XRD patterns of Fe_3O_4/GO nanocomposite before and after calcination (Fe_3O_4/RGO).

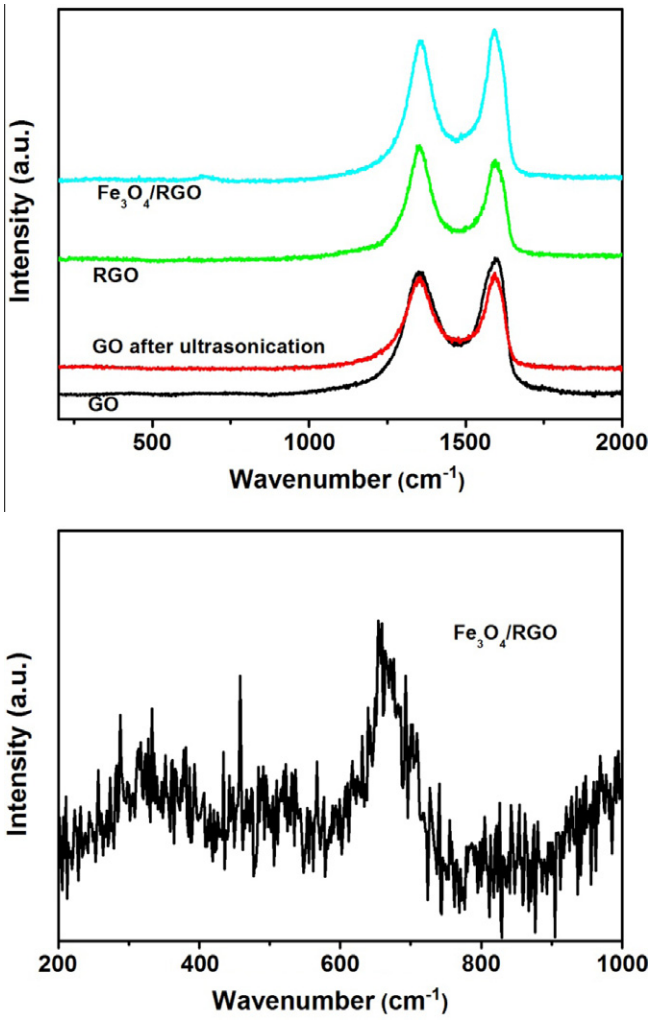

Fig. 2. Raman spectra of the resultant GO, RGO and Fe_3O_4/RGO nanocomposite and GO after ultrasonication as a comparison. The inset shows an enlargement of Fe_3O_4/RGO at low wavenumber region.

at 655, 310 and 516 cm^{-1} correspond to one A1 g mode and two Eg modes of Fe_3O_4 in Fe_3O_4/RGO, respectively. Similar absorptions were observed for neat Fe_3O_4 (670, 300 and 530 cm^{-1} from literature) [29] with shifts of 15, 10 and 14 cm^{-1}, possibly due to the interaction between Fe_3O_4 and RGO.

SEM micrographs of RGO and Fe_3O_4/RGO are compared in Fig. 3. Layer-structured RGO shows smooth surface (Fig. 3a–c), while Fe_3O_4/RGO exhibits a number of wrinkles (Fig. 3d–f) and nanoscale textures, indicative of a much rougher surface (Fig. 3d). A large number of Fe_3O_4 nanoparticles are observed clearly on the RGO surface with no aggregation (Fig. 3e), indicating a good interaction between nanoparticles and RGO. Fig. 3f shows a uniform dispersion of these particles with tens of nanometer in diameter, illustrating the effectiveness of our method in fabricating size-controlled Fe_3O_4 nanoparticles and dispersing them homogeneously on the RGO surface. It is noteworthy that the size distribution of the nanoparticles is narrowly centered at ~25 nm (Fig. 3g).

Fig. 4 further characterizes the structure and composition of Fe_3O_4/RGO using transmission electron microscopy (TEM) and energy-dispersive X-ray measurement (EDX). At low magnifications (Fig. 4a–c), many nanoparticles are found to uniformly disperse on corrugated graphene layers; at high magnifications, no aggregation can be detected and the particle size was measured as 30–40 nm by randomly selecting 40 particles, corresponding to what

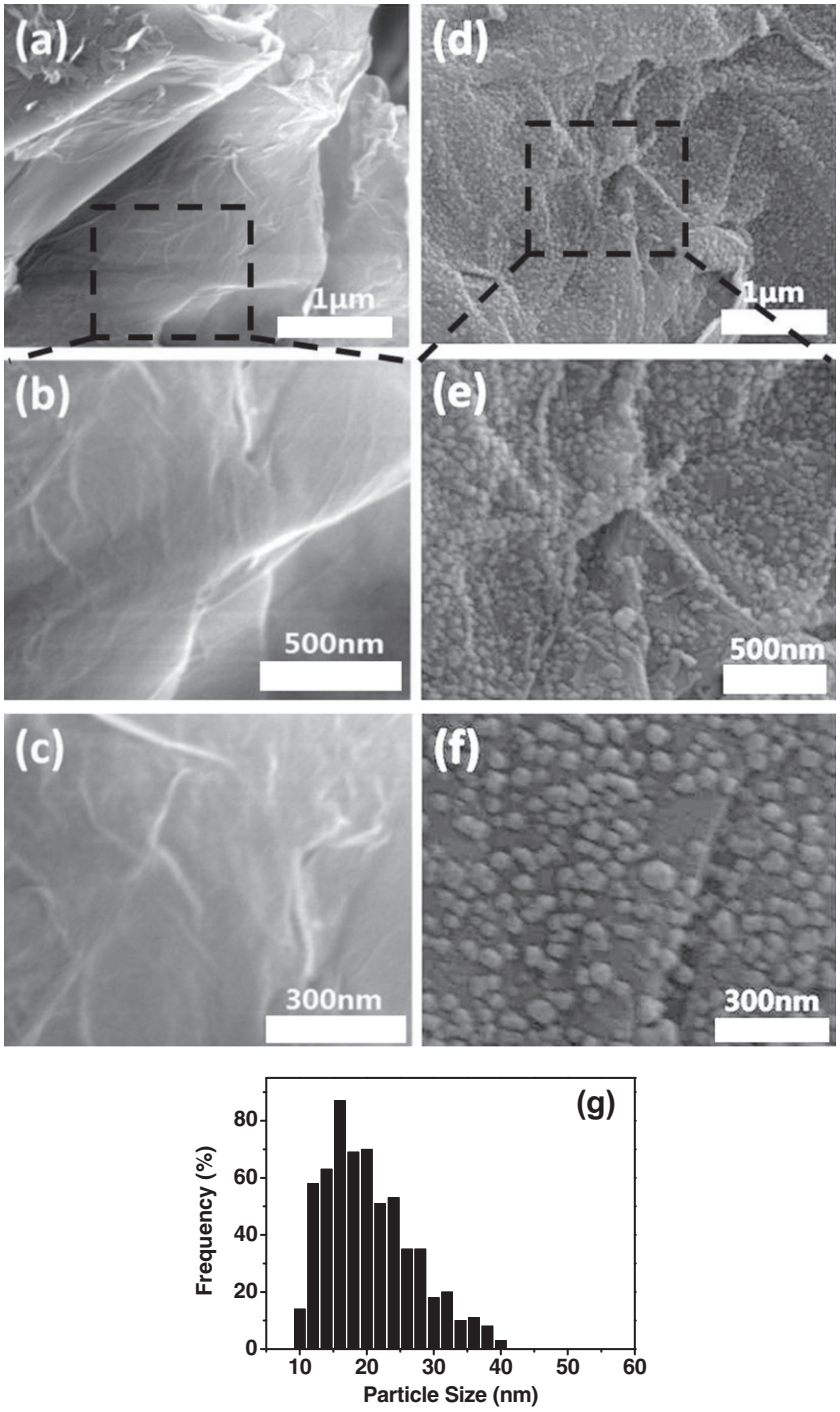

Fig. 3. FE-SEM images of reduced RGO (a–c) and Fe_3O_4/RGO nanocomposite (d–f) at different magnifications, (g) the measured particle size distribution.

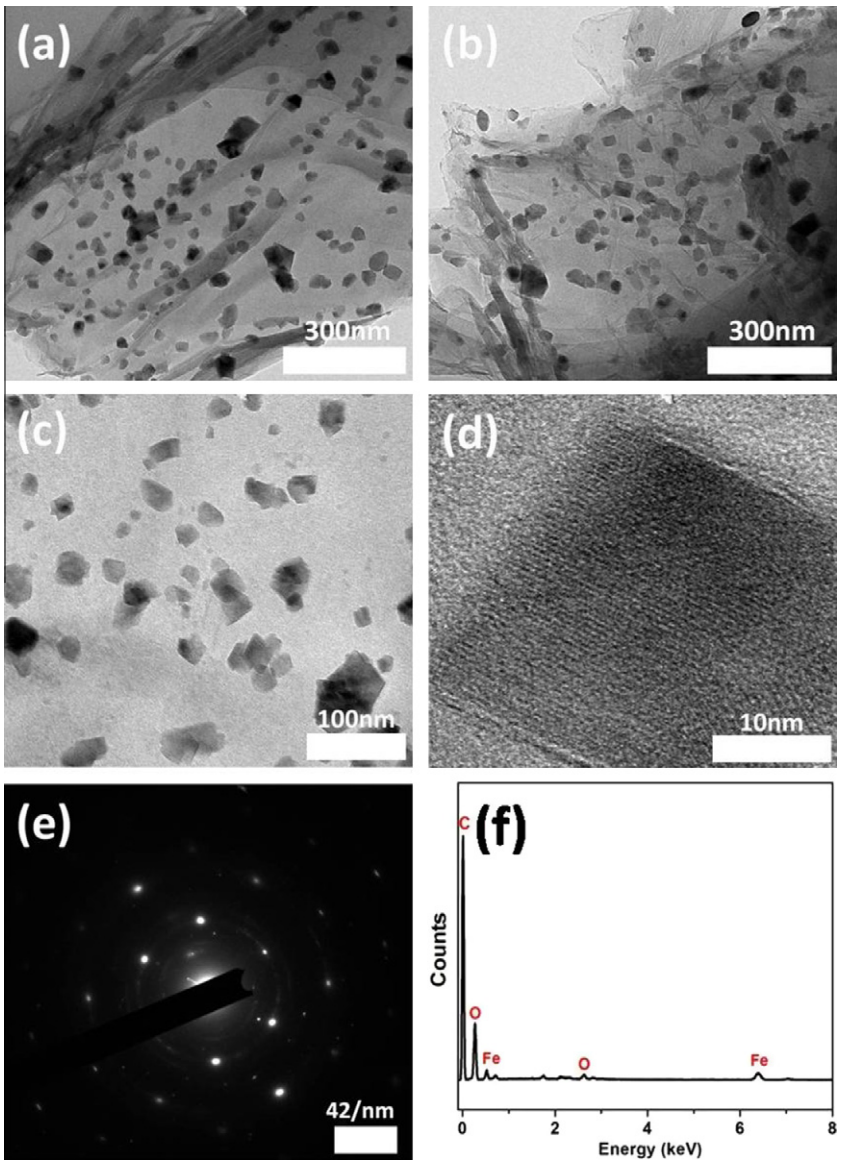

Fig. 4. TEM images of Fe_3O_4/RGO nanocomposite at different resolutions (a–d) and the SAED images and the corresponding EDX.

we calculated in our foregoing wide-angle XRD analysis. As demonstrated in Fig. 4d, the measured lattice spacing values of 0.48 and 0.29 nm correspond to (111) and (202) planes of Fe_3O_4, respectively. The selected area electron diffraction (SAED) pattern (Fig. 4e) indicates a high crystalline nature of the magnetite (JCPDF 75-0033). Typical EDX pattern indicates that Fe_3O_4/RGO contains Fe_3O_4 and C elements.

There must be a reasonably strong interaction between Fe_3O_4 nanoparticles and RGO; otherwise, these nanoparticles would aggregate. A Fourier transform infrared spectrometer was adopted to identify this interaction. In Fig. 5, GO shows obvious absorptions at 1220.1 and 1606.3 cm^{-1} corresponding to C–O functionalities such as COOH and the sp^2 hybridized structure, respectively. Through thermal treatment, the absorptions of GO at 1724.8 (COOH), 1383.3–1055.3 (COC/COH) and 591.2 cm^{-1} either disappear or largely reduce due to the elimination of most oxygenous groups from GO. As for Fe_3O_4/RGO, the broad absorptions at low frequencies are ascribed to the vibration of Fe–O bond ($\sim$635 cm^{-1}) which was not observed in the spectrum of GO. The skeletal vibration of the RGO sheets at 1569.6 cm^{-1} was also clearly observed for Fe_3O_4/RGO, illustrating its existence. The

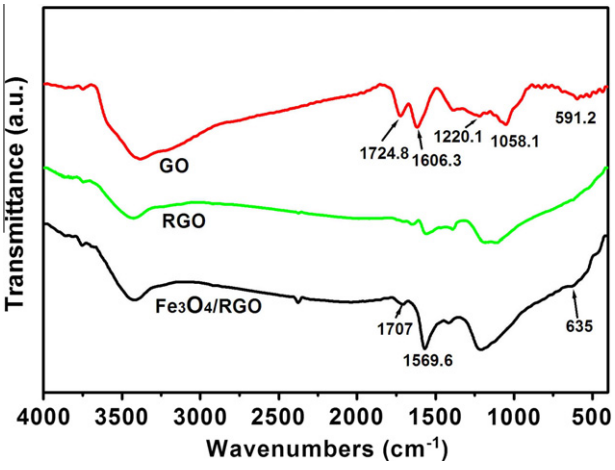

Fig. 5. FT-IR spectra of GO and RGO and Fe_3O_4/RGO nanocomposite.

absorption at 1724.8 cm^{-1} corresponding to C = O of –COOH on the GO shifts to 1707 cm^{-1} due to the formation of –COO after coating with Fe_3O_4. The characteristic absorption corresponding

to the stretching vibration of Fe–O bond is also shifted to higher wavenumber of 635 cm^{-1} compared to that of 570 cm^{-1} reported for the stretching mode of Fe–O in bulk Fe_3O_4, suggesting that Fe_3O_4 is bound to the –COO on the GO surface [21,30]. The 3400 cm^{-1} absorption in all the three cases is contributed to the vibration of –OH in H_2O.

XPS was conducted to further investigate the formation of Fe_3O_4 in Fe_3O_4/RGO. Fig. 6 shows a Fe2p spectrum of Fe_3O_4/RGO. Distinct peaks at 710.7 and 724 eV (Fig. 6a) indicates the existence of Fe^{3+} in Fe_3O_4/RGO. The presence of Fe^{2+} in Fe_3O_4/RGO is indicated by the disappearance of the satellite peak at around 718 eV between the two main Fe2p peaks. Therefore the obtained Fe_3O_4/RGO consists of almost pure magnetite.

TGA should explain the strong interaction between nanoparticles and RGO. Fig. 7 shows TGA graphs of RGO and Fe_3O_4/RGO by treating in air from 40 to 900 °C. The largest weight loss occurs from 520 to 600 °C for both RGO and Fe_3O_4/RGO, due to oxidation in air. While the remaining RGO is lower than 5 wt.%, the weight loss of Fe_3O_4/RGO is stabilized at ~80 wt.% at 600–900 °C, indicating that ~20 wt.% of Fe_3O_4/RGO belongs to Fe_3O_4 nanoparticles. The 20 wt.% gradual loss of RGO from 150 to 500 °C is mainly due to the removal of oxygen-containing functional groups on the surface of RGO; by contrast, Fe_3O_4/RGO is fairly stable since no obvious loss seen until 500 °C. This means that the combination of RGO with Fe_3O_4 nanoparticle provides more thermal stability, implying a strong interaction between them.

Fig. 8 shows magnetic hysteresis loops of Fe_3O_4/RGO measured at room temperature. The obviously low hysteresis reveals that our magnetic nanoparticles were nearly super paramagnetic; that is, no remanence remains when the applied magnetic field is removed. A saturation magnetization (*Ms*) of 30 emu/g is found, significantly lower than that (84.5 emu/g) measured from a commercial magnetite fine powder [31]. The low *Ms* is explained by size-dependent magnetization of the magnetic nanoparticles, as supported by previous work [32,33].

3.2. Proposed mechanism

GO is known to consist of oxidized graphene sheets that have their basal planes decorated with epoxide and hydroxyl groups, in addition to a few carboxyl groups. Carboxylic moieties can interact with the metal cations through physisorption, electrostatic binding. Thus, Fe^{3+} ions can attach to the carboxyl groups of GO, and then react with O_2 through the thermal treatment to produce FeOOH or $Fe(OH)_2$ on the surface of the exfoliated sheets as evidenced by XRD, Raman and FT-IR analysis. However, the number

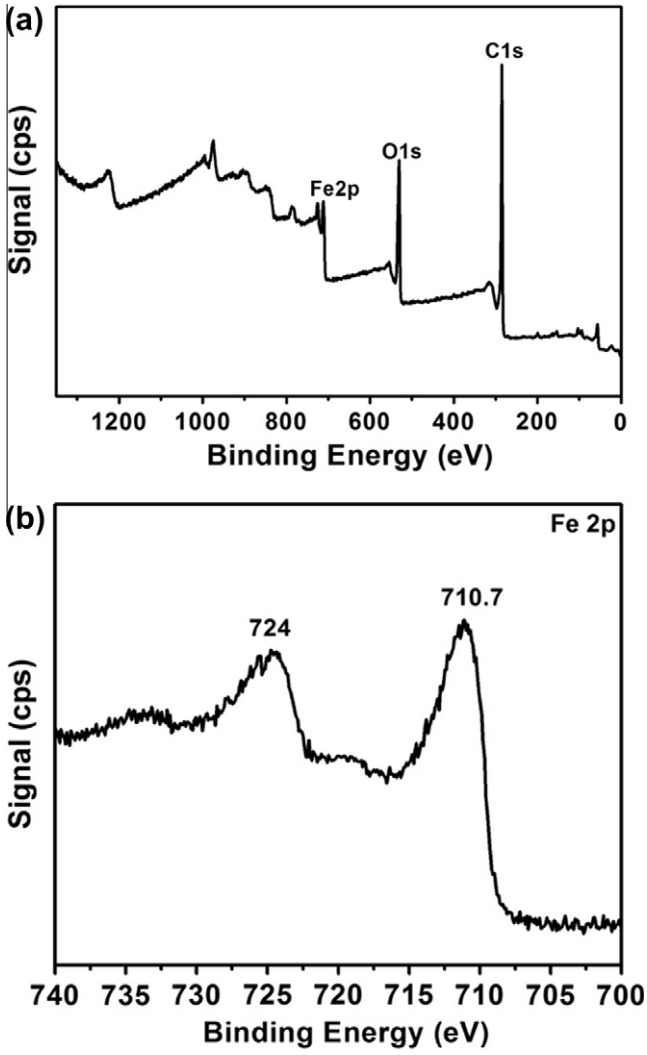

Fig. 6. The survey XPS spectrum of Fe_3O_4/RGO nanocomposite and the corresponding Fe 2p spectrum.

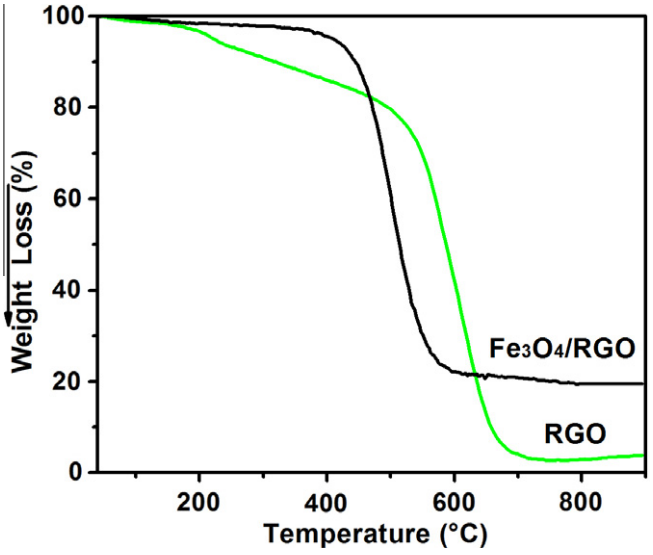

Fig. 7. TGA curves of RGO and Fe_3O_4/RGO, the heating rate used is 20 °C/min.

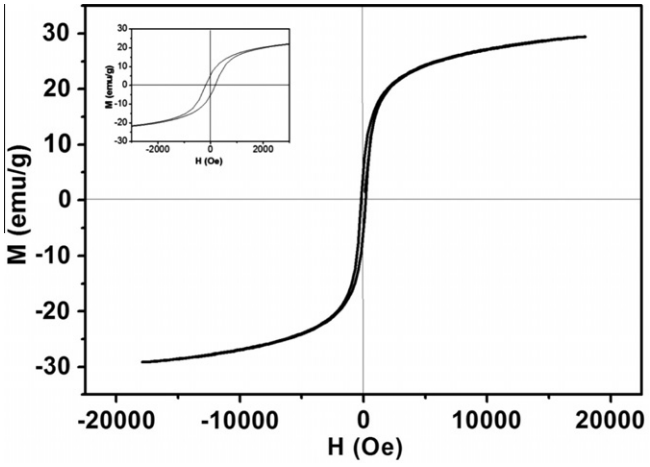

Fig. 8. Magnetization curve of reduced Fe_3O_4/RGO composite.

of ionizable carboxyl groups at the edge is not sufficient to complex the metal cations and to stabilize the metal oxide particles formed, often resulting in less homogeneous and larger particles. Therefore, surface functionalization is generally needed to produce a homogeneous particle dispersion.

Herein our novel process employs no surface modification, but leads to fine Fe_3O_4 nanoparticles that uniformly dispersed on the RGO surface. This is explained by the effect of ultrasonication [18,19]. It is known that size control must be performed within a very short nucleation period and the final particle number does not change during the particle growth. When the precursor solution is exposed to ultrasound irradiation, extremely-high temperatures and pressures are created during acoustic cavitation, providing energy to generate Fe_3O_4 nuclei. Meanwhile, the produced high temperature and the adsorbed bubbling gases on nuclei surface reduce the interfacial free energy between nuclei and solution, consequently inhibiting the growth of particles. Accordingly, a much more rapid nucleation followed with a slower grain growth leads to smaller particle sizes in the process. Moreover, the collapse of the bubbles drives high-speed jets of liquid into the solid surface, promoting the attachment of the newly-formed nanoparticles to the GO surface. That is the reason why a uniform dispersion of fine Fe_3O_4 particles has been achieved in our fabrication.

3.3. Electrochemical performance of the biosensor

It is well known that proteins and enzymes containing heme-groups, such as horseradish peroxidase, cytochrome c, hemoglobin and myoglobin, can reduce O_2 and H_2O_2 electro-catalytically. In order to estimate the electrochemical catalytic activity of Fe_3O_4/RGO combined with hemoglobin (Hb) for reduction of O_2 and H_2O_2, a current response measurement was performed on the electrodes modified by our Fe_3O_4/RGO and Hb in presence of H_2O_2 (Fig. 9).

For an electrode modified by RGO only, almost no response was observed. Although either Fe_3O_4/RGO or RGO-Hb just marginally improves the current response, Fe_3O_4/RGO/Hb demonstrates a significant improvement. The reason can be explained as below: Fe_3O_4 nanoparticles are known for readily adsorbing H_2O_2 molecules, the ions Fe^{2+} or Fe^{3+} in Fe_3O_4 can react with H_2O_2 and then produce radical species through the surface Fenton reactions [37]. Since the intact Fe_3O_4 nanoparticles contribute to the catalytic breakdown of H_2O_2, the surface properties and chemical compositions of these nanoparticles play a critical role in the peroxidase-like catalysis. A favorable Fe_3O_4 catalyst should be capable to disperse uniformly on a carrier for an effective interaction with H_2O_2. Our uniformly dispersed Fe_3O_4 nanoparticles on RGO sheets, made by ultrasonication, are indeed beneficial to the high biosensor performance. Meanwhile, Hb itself can reduce O_2 and H_2O_2 electrocatalytically. Moreover, the reduced graphene oxide sheets not only act as a matrix to disperse Fe_3O_4 but promote the electron transfer between the peroxide and electrode surface. Therefore, the high performance of Fe_3O_4/RGO/Hb for H_2O_2 detection is attributed to the synergistic effects of the Fe_3O_4 nanoparticles, the reduced graphene oxide sheets and the electrocatalytically reduction of O_2 and H_2O_2 by Hb.

Fig. 10 illustrates the cyclic voltammograms of Fe_3O_4/RGO/Hb-modified electrode with and without H_2O_2. In Fig. 10a, a pair of ill-defined redox peaks is observed for the Fe_3O_4/RGO/Hb-modified electrode. An anodic peak potential and a cathodic peak potential are located at −0.129 and −0.306 V, respectively, a characteristic of the Hb-heme Fe(III)/Fe(II) redox couple. With addition of H_2O_2, the cathodic peak current increases obviously, indicating that the the Fe_3O_4/RGO/Hb-modified electrode promotes the electro-catalytic reduction of H_2O_2.

The amperometric response of the Fe_3O_4/RGO/Hb-modified biosensor was investigated by successive addition of H_2O_2 under an optimized condition (Fig. 11a). When different concentrations of H_2O_2 were added into the buffer solution, the reductive current rises steeply to reach a stable value. The enzyme electrode achieved 95% the steady-state current within 10 s. The amperometric current increases linearly with H_2O_2 concentration from 4×10^{-6} to 1×10^{-3} M with a detection limit of 2×10^{-6} M at a signal/noise ratio 3 ($S/N = 3$) (Fig. 11b), which is an order lower than that (2.1×10^{-5} M) of a previous H_2O_2 biosensor based on a chitosan/Fe_3O_4/Hb-modied electrode [34]. The regression equation was expressed as $i_p(\mu A) = -0.0468\ C(\mu M) - 0.9956$ ($R^2 = 0.9937$). The sensitivity was 0.0468 μA μM^{-1}.

The apparent Michaelis–Menten constant (K_M^{app}), an indication of the enzyme substrate kinetics for the biosensor, can be calculated from the electrochemical version of the Lineweaver–Burk equation [35]:

$$\frac{1}{I_{ss}} = \frac{1}{I_{max}} + \frac{K_M^{app}}{I_{max}^C}$$

where I_{ss} is the steady-state current after addition of substrate, C the bulk concentration of substrate and I_{max} the maximum current in a saturated substrate solution. K_M^{app} can be obtained by analyzing slope and intercept of the plot of reciprocals of the steady-state current vs. H_2O_2 concentration. The smaller K_M^{app}, the higher the cata-

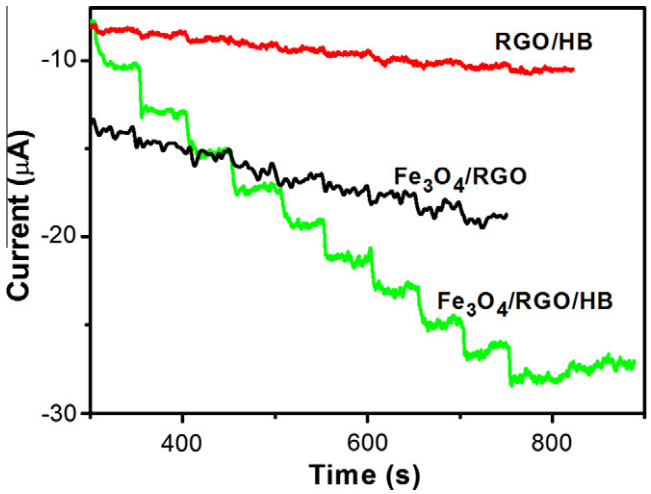

Fig. 9. Current responses of various modified electrodes to H_2O_2.

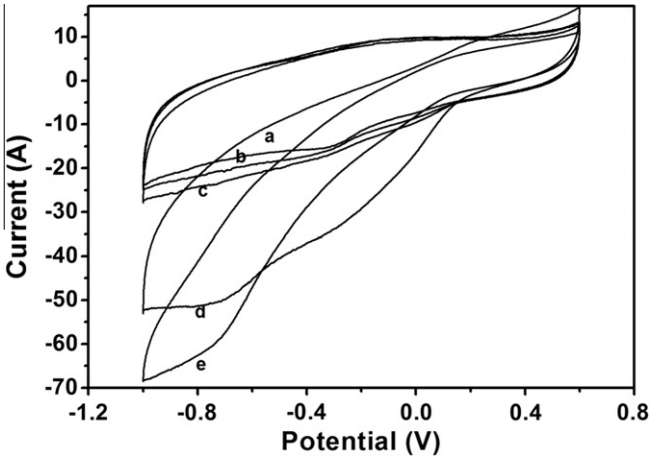

Fig. 10. Cyclic voltammograms of Fe_3O_4/RGO/Hb-modified electrode in 0.1 M pH 7.0 PBS without H_2O_2 (a), 1×10^{-5} M H_2O_2 (b),1×10^{-4} M H_2O_2 (c), 1×10^{-3} M H_2O_2 (d) and 5×10^{-3} H_2O_2 (e) at a scan rate of 100 mV s^{-1}.

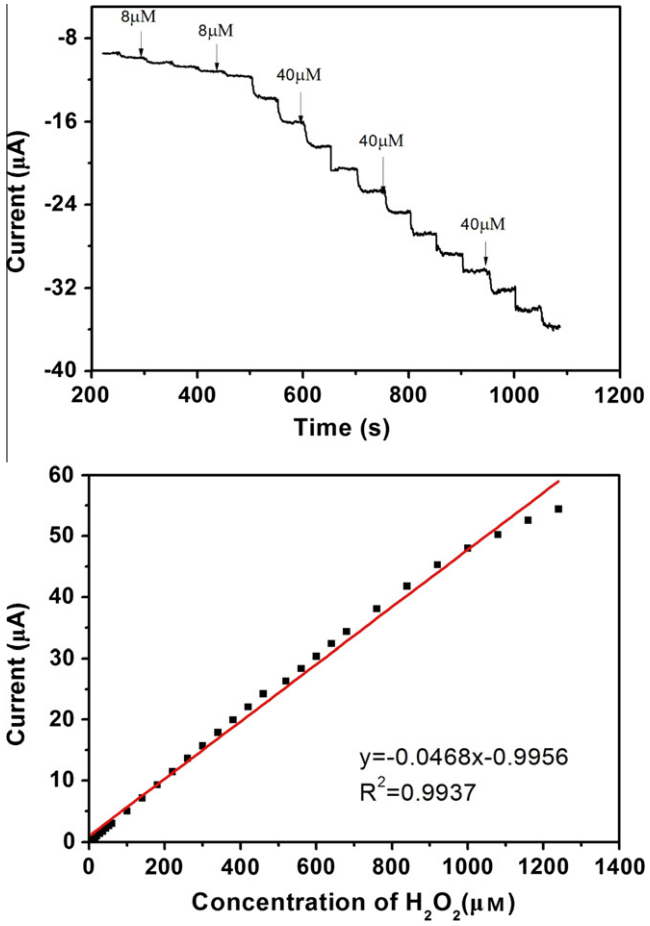

Fig. 11. Current-time responses of Fe_3O_4/RGO/Hb-modified electrode to successive additions of the various concentrations of H_2O_2. Inset: the plot of the reduction current vs. H_2O_2 concentration. The applied potential was −0.4 V.

lytic ability it is. The K_M^{app} value in this work was calculated to be 1.1 mM, far smaller than a recent K_M^{app} value 2.3 mM measured from a Hb/Au/Fe_3O_4-modified electrode [36], and this means that our Fe_3O_4/RGO/Hb possesses a higher affinity for H_2O_2.

4. Conclusions

A Fe_3O_4/RGO nanocomposite was fabricated by a sonochemical method that produced Fe_3O_4 nanoparticles of 30–40 nm in diameter, which uniformly dispersed on the graphene surface. Our Fe_3O_4/RGO was immobilized with Hb to fabricate a biosensor for detecting H_2O_2. The biosensor demonstrated a fast response of H_2O_2 less than 10 s and an excellent linear relationship at 4×10^{-6}–1×10^{-3} M with the detection limit of 2×10^{-6} M ($S/N = 3$). Fe_3O_4/RGO not only provides a biocompatible microenvironment for the immobilized biomolecules but promotes a direct electron transfer between electrode and peroxide. Due to the magnetic property of Fe_3O_4 nanoparticles, Fe_3O_4/RGO can be readily manipulated by an external magnetic field, and this facilitates the electrode modification and the recycling of used products. This strategy of cost-effective fabrication of Fe_3O_4/RGO would provide a platform for the development of a wide variety of graphene-metal oxide nanocomposite to construct high-performance biosensors.

Acknowledgments

The authors gratefully acknowledge financial support for this research from the Morgan Crucible Company, the National Science Foundation of China (Nos. 51072117, 51171110), National Basic Research Program of China (973 Program, 2012CB619600), Shanghai Science and Technology Committee (No. 10JC1407600). We also thank the Shanghai Jiao Tong University (SJTU) Instrument Analysis Center for the measurements.

References

[1] D. Moscone, D. D'Ottavi, D. Compagnone, G. Palleschi, A. Amine, Construction and analytical characterization of prussian-blue-based carbon paste electrodes and their assembly as oxidase enzyme sensors, Anal. Chem. 73 (2001) 2529–2535.
[2] X. Kang, J. Wang, H. Wu, I.A. Aksay, J. Liu, Y. Lin, Glucose oxidase-graphene-chitosan modified electrode for direct electrochemistry and glucose sensing, Biosens. Bioelectron. 25 (2009) 901–905.
[3] S. Alwarappan, S. Prabhulkar, A. Durygin, C.Z. Li, The effect of electrochemical pretreatment on the sensing performance of single walled carbon nanotubes, J. Nanosci. Nanotechnol. 9 (2009) 2991–2996.
[4] X. Chen, C. Fu, W. Yang, Graphite nanosheet-based composites for mediator-free H_2O_2 biosensor, The Anal. 134 (2009) 2135–2140.
[5] A.K. Kafi, G. Wu, A. Chen, A novel hydrogen peroxide biosensor based on the immobilization of horseradish peroxidase onto Au-modified titanium dioxide nanotube arrays, Biosens. Bioelectron. 24 (2008) 566–571.
[6] A. Salimi, E. Sharifi, A. Noorbakhsh, S. Soltanian, Direct voltammetry and electrocatalytic properties of hemoglobin immobilized on a glassy carbon electrode modified with nickel oxide nanoparticles, Electrochem. Commun. 8 (2006) 1499–1508.
[7] G.L. Luque, M.C. Rodríguez, G.A. Rivas, Glucose biosensors based on the immobilization of copper oxide and glucose oxidase within a carbon paste matrix, Talanta 66 (2005) 467–471.
[8] Y.L. Liu, Y.H. Yang, H.F. Yang, Z.M. Liu, G.L. Shen, R.Q. Yu, Nanosized flower-like ZnO synthesized by a simple hydrothermal method and applied as matrix for horseradish peroxidase immobilization for electro-biosensing, J. Inorg. Biochem. 99 (2005) 2046–2053.
[9] E. Topoglidis, C.J. Campbell, A.E.G. Cass, J.R. Durrant, Nitric oxide biosensors based on the immobilization of hemoglobin on mesoporous titania electrodes, Electroanalysis 18 (2006) 882–887.
[10] G. Zhao, J.-J. Feng, J.-J. Xu, H.-Y. Chen, Direct electrochemistry and electrocatalysis of heme proteins immobilized on self-assembled ZrO_2 film, Electrochem. Commun. 7 (2005) 724–729.
[11] E. Katz, I. Willner, Biomolecule-functionalized carbon nanotubes: applications in nanobioelectronics, Chem. Phys. Chem: A Eur. J. Chem. Phys. Phys. Chem. 5 (2004) 1084–1104.
[12] E. Katz, L. Sheeney-Haj-Ichia, I. Willner, Electrical contacting of glucose oxidase in a redox-active rotaxane configuration, Angew. Chem. Int. Ed. Engl. 43 (2004) 3292–3300.
[13] L.M. Rossi, A.D. Quach, Z. Rosenzweig, Glucose oxidase-magnetite nanoparticle bioconjugate for glucose sensing, Anal. Bioanal. Chem. 380 (2004) 606–613.
[14] J. Hrbac, C. Gregor, M. Machova, J. Kralova, T. Bystron, M. Ciz, A. Lojek, Nitric oxide sensor based on carbon fiber covered with nickel porphyrin layer deposited using optimized electropolymerization procedure, Bioelectrochemistry 71 (2007) 46–53.
[15] G. Zhou, D.-W. Wang, F. Li, L. Zhang, N. Li, Z.-S. Wu, L. Wen, G.Q. Lu, H.-M. Cheng, Graphene-wrapped Fe_3O_4 anode material with improved reversible capacity and cyclic stability for lithium ion batteries, Chem. Mater. 22 (2010) 5306–5313.
[16] M. Zhang, D. Lei, X. Yin, L. Chen, Q. Li, Y. Wang, T. Wang, Magnetite/graphene composites: microwave irradiation synthesis and enhanced cycling and rate performances for lithium ion batteries, J. Mater. Chem. 20 (2010) 5538–5543.
[17] C.-T. Hsieh, J.-Y. Lin, C.-Y. Mo, Improved storage capacity and rate capability of Fe_3O_4/graphene anodes for lithium-ion batteries, Electrochim. Acta 58 (2011) 119–124.
[18] S.K. Behera, Enhanced rate performance and cyclic stability of Fe_3O_4-graphene nanocomposites for Li ion battery anodes, Chem. Commun. 47 (2011) 10371–10373.
[19] K. Zhou, Y. Zhu, X. Yang, C. Li, Preparation and application of mediator-free H_2O_2 biosensors of graphene-Fe_3O_4 composites, Electroanalysis 23 (2011) 862–869.
[20] Q.H. Le, H.C. Kuan, J.B. Dai, J. Ma, Structure-property relations of 55 nm particle-toughened epoxy, Polymer 51 (2010) 4867–4879.
[21] X. Yang, X. Zhang, Y. Ma, Y. Huang, Y. Wang, Y. Chen, Superparamagnetic graphene oxide-Fe_3O_4 nanoparticles hybrid for controlled targeted drug carriers, J. Mater. Chem. 19 (2009) 2710–2714.
[22] F. He, J. Fan, D. Ma, L. Zhang, C. Leung, H.L. Chan, The attachment of Fe_3O_4 nanoparticles to graphene oxide by covalent bonding, Carbon 48 (2010) 3139–3144.
[23] A. Gedanken, X. Tang, Y. Wang, N. Perkas, Y. Koltypin, M.V. Landau, L. Vradman, M. Herskowitz, Using sonochemical methods for the preparation of mesoporous materials and for the deposition of catalysts into the mesopores, Chem. – A Eur. J. 7 (2001) 4546–4552.
[24] P. Jeevanandam, Y. Koltypin, O. Palchik, A. Gedanken, Synthesis of morphologically controlled lanthanum carbonate particles using ultrasound irradiation, J. Mater. Chem. 11 (2001) 869–873.

[25] T.J. Mason, J.P. Lorimer, D.M. Bates, Quantifying sonochemistry: casting some light on a 'black art', Ultrasonics 30 (1992) 40–42.
[26] W. Thamjaree, W. Nhuapeng, T. Tunkasiri, Analysis of X-ray diffraction line profiles of lead zirconate titanate using the fourier method, Ferroelectr. Lett. 31 (2004) 79–85.
[27] H.F. Chen, G.D. Wei, X. Han, S. Li, P.P. Wang, M. Chubik, A. Gromov, Z.P. Wang, W. Han, Large-scale synthesis of hierarchical alpha-FeOOH flowers by ultrasonic-assisted hydrothermal route, J. Mater. Sci.: Mater. Electron. 22 (2011) 252–259.
[28] Y. Wang, X. Chen, Y. Zhong, F. Zhu, K.P. Loh, Large area, continuous, few-layered graphene as anodes in organic photovoltaic devices, Appl. Phys. Lett. 95 (2009) 063302.
[29] D.L.A. de Faria, S.V. Silva, M.T. de Oliveira, Raman microspectroscopy of some iron oxides oxyhydroxides, J. Raman Spectrosc. 28 (1997) 873–878.
[30] J. Guo, S. Zhu, Z. Chen, Y. Li, Z. Yu, Q. Liu, J. Li, C. Feng, D. Zhang, Sonochemical synthesis of TiO(two nanoparticles on graphene for use as photocatalyst, Ultrason. Sonochem. 18 (2011) 1082–1090.
[31] M. Chen, J.P. Liu, S. Sun, One-step synthesis of FePt nanoparticles with tunable size, J. Am. Chem. Soc. 126 (2004) 8394–8395.
[32] I. Morjan, R. Alexandrescu, F. Dumitrache, R. Birjega, C. Fleaca, I. Soare, C.R. Luculescu, G. Filoti, V. Kuncer, L. Vekas, N.C. Popa, G. Prodan, V. Ciupina, Iron oxide-based nanoparticles with different mean sizes obtained by the laser pyrolysis: structural and magnetic properties, J. Nanosci. Nanotechnol. 10 (2010) 1223–1234.
[33] S. Laurent, J.L. Bridot, L.V. Elst, R.N. Muller, Magnetic iron oxide nanoparticles for biomedical applications, Future Med. Chem. 2 (2010) 427–449.
[34] G.S. Lai, H.L. Zhang, D.Y. Han, A novel hydrogen peroxide biosensor based on hemoglobin immobilized on magnetic chitosan microspheres modified electrode, Sens. Actuators, B 129 (2008) 497–503.
[35] J. Li, S.N. Tan, H. Ge, Silica sol-gel immobilized amperometric biosensor for hydrogen peroxide, Anal. Chim. Acta 335 (1996) 137–145.
[36] C.M. Yu, J.W. Guo, H.Y. Gu, Direct electrochemical behavior of hemoglobin at surface of Au@Fe_3O_4 magnetic nanoparticles, Microchim. Acta 166 (2009) 215–220.
[37] N. Wang, L. Zhu, D. Wang, M. Wang, Z. Lin, H. Tang, Sono-assisted preparation of highly-efficient peroxidase-like Fe_3O_4 magnetic nanoparticles for catalytic removal of organic pollutants with H_2O_2, Ultrason. Sonochem. 17 (2010) 526–533.